Sideroflexins enable mitochondrial transport of polar neutral amino acids

Samuel Block[1,2,3], Fangtao Chi[1], Paul C. Rosen[2], S. Sebastian Pineda[4,5,6,7], Alicia M. Darnell[1,2,8], Keene L. Abbott[1,2], Izabella A. Pena[6,9], Myriam Heiman[6,9], Ömer H. Yilmaz[1,2,10,11], Nora Kory[3,7,12,*], Matthew G. Vander Heiden[1,2,7,12,*]

[1]David H. Koch Institute for Integrative Cancer Research, MIT, Cambridge, MA, USA

[2]Department of Biology, MIT, Cambridge, MA, USA

[3]Department of Molecular Metabolism, Harvard T.H. Chan School of Public Health, Boston, MA, USA

[4]Department of Electrical Engineering and Computer Science, Massachusetts Institute of Technology, Cambridge, MA 02139, USA

[5]Computer Science and Artificial Intelligence Laboratory, Massachusetts Institute of Technology, Cambridge, MA 02139, USA

[6]Picower Institute for Learning and Memory, MIT, Cambridge, MA, USA

[7]Broad Institute of MIT and Harvard, Cambridge, MA 02141, USA

[8]Department of Pharmacology and Cancer Biology, Duke University School of Medicine, Durham, NC, USA

[9]Department of Brain and Cognitive Sciences, MIT, Cambridge, MA, USA

[10]Department of Pathology, Massachusetts General Hospital and Harvard Medical School, Boston, MA, USA

[11]Department of Pathology, Beth Israel Deaconess Hospital and Harvard Medical School, Boston, MA, USA

[12]Dana-Farber Cancer Institute, Boston, MA, USA

[*]Correspondence: mvh@mit.edu, nkory@hsph.harvard.edu

Abstract: Mitochondria contribute to compartmentalized metabolism in eukaryotic cells, supporting key enzymatic reactions for cell function and energy homeostasis. However, this compartmentalization necessitates regulated metabolite transport across mitochondrial membranes. Although many transport proteins have been identified, several mitochondrial amino acid transporters remain largely uncharacterized. Using CRISPR-Cas9–mediated candidate transporter knockouts coupled with assessment of metabolite transport via a mitochondrial swelling assay, we identify SFXN1, previously characterized for its role in mitochondrial serine transport, as a protein that mediates mitochondrial transport of a range of other polar neutral amino acids including proline, glycine, threonine, taurine, hypotaurine, β-alanine, and γ-

aminobutyric acid (GABA). Furthermore, the SFXN1 paralogues SFXN2 and SFXN3 partially complement loss of SFXN1 to enable glycine transport, while SFXN2 and SFXN5 partially complement loss of SFXN1 to enable GABA transport. Altogether, these data suggest that sideroflexins facilitate the transport of polar neutral amino acids across the inner mitochondrial membrane.

Introduction

Amino acid transport proteins with molecular specificity enable transport across the inner mitochondrial membrane (*1*). Aside from likely supplying amino acids for the synthesis of proteins encoded by the mitochondrial genome, which are critical for respiration and mitochondrial ATP synthesis (*2*, *3*), mitochondrial transport of amino acids affects many metabolic pathways that are often altered in disease. For example, mitochondrial proline export is upregulated in cancer-associated fibroblasts to support collagen synthesis, which promotes tumor growth and metastasis (*4*), while impaired mitochondrial proline import and degradation leads to synaptic dysfunction (*5*) and is associated with schizophrenia and hyperprolinemia (*6*). Non-proteinogenic amino acids are also involved in metabolic pathways that cross mitochondrial membranes, such as the degradation of the inhibitory neurotransmitter γ-aminobutyric acid (GABA) within glial mitochondria (*7*). While a number of mitochondrial amino acid transporters belonging mainly to the SLC25 protein family have been identified (*8*, *9*), the mitochondrial transporters for proline, methionine, alanine, cysteine, threonine, asparagine, phenylalanine, tyrosine, tryptophan, and many non-proteinogenic amino acids including GABA, taurine, and β-alanine remain unknown. Many of these amino acids are relatively polar and neutral at physiological pH, and despite data generated nearly 50 years ago suggesting the existence of a mitochondrial carrier with broad specificity for polar neutral amino acids (*10*, *11*), no such carrier has been reported in humans. To address this, we used CRISPR-Cas9 gene editing to delete candidate mitochondrial transporters and assessed how this affects mitochondrial uptake of amino acids using a mitochondrial swelling assay. This approach identified SFXN1 as a regulator of mitochondrial permeability to proline, and together with supporting metabolic studies suggest that sideroflexins enable transport of the polar neutral amino acids glycine, threonine, taurine, hypotaurine, β-alanine, and GABA across the inner mitochondrial membrane.

Results

A targeted swelling screen identifies SFXN1 as a regulator of mitochondrial proline permeability

Studies using isolated mitochondria from non-human organisms have provided evidence for the existence of a mitochondrial proline transporter (*10*, *12–14*), but the molecular identity of that transporter and whether such a transporter exists in humans remains unknown. To determine if humans contain a mitochondrial proline transporter, we isolated mitochondria from HEK293T cells and measured the kinetics of proline uptake using mitochondrial swelling, a well-established transport assay used to assess the properties of many mitochondrial metabolite carriers (*15–18*) (Fig. 1A). Compared to sucrose, which does not penetrate the inner mitochondrial membrane, we observed robust swelling with proline (Fig. S1A), including a preference for the physiological L isomer (Fig. 1B-C). These data suggest that purified

mitochondria with an intact inner membrane contain a proline transporter, since both isomers would elicit equal responses if swelling occurred by diffusion, consistent with studies using mitochondria isolated from rat (*10*), yeast (*13*) and plants (*12*).

To screen for mitochondrial proline transporters, we used CRISPR-Cas9 gene editing (*19*) to individually delete 10 candidate mitochondrial transporters and compared how loss of each candidate affects mitochondrial proline swelling relative to non-targeting control (NTC) (Fig. 1D). In this screen, we considered members of the SFXN protein family (SFXN1-5) and SLC25A38, which have been shown to transport other small neutral amino acids (*9*, *20*), as well as SLC25A16, SLC25A30, SLC25A35, and SLC25A53 which are the four uncharacterized putative mitochondrial transporters we found to be expressed in HEK293T cells by proteomics (Fig. S1B). Of note, mitochondria isolated from cells expressing a sgRNA targeting SFXN1, but not mitochondria isolated from cells expressing a sgRNA targeting any of the other selected transporters, demonstrated reduced swelling with proline compared to NTC (Fig. 1D). To validate that loss of SFXN1 reduces proline swelling, we generated clonal SFXN1 knockout HEK293T and K562 cell lines (Fig. S1C-D). Mitochondria isolated from these cells also showed reduced swelling with proline (Fig. 1E, Fig. S1E), which was rescued by re-expression of SFXN1 but not overexpression of any other SFXN protein (SFXN2-5) (Fig. 1F). To assess the stereospecificity of this effect, we also performed swelling with D-proline, which was unaltered with loss of SFXN1 (Fig. 1G).

Loss of SFXN1 inhibits mitochondrial proline export

Proline can be synthesized in the cytosol through PYCR3 or within mitochondria through PYCR1 or PYCR2 (*21*), and glutamine is a carbon source for mitochondrial proline synthesis in cultured mammalian cells (*22*) (Fig. 2A). However, recent studies have shown that mitochondrial proline synthesis is required to maintain adequate cellular proline levels for proliferation (*23*, *24*). To determine if the reduction in mitochondrial proline permeability we observe in SFXN1 knockout mitochondria is associated with impaired export of mitochondrially-synthesized proline from glutamine, we incubated HEK293T cells with $^{13}C_5$-L-glutamine and measured proline released into the media by liquid chromatography-mass spectrometry (LC-MS). For comparison, we also generated cells lacking various combinations of PYCR1-3 (Fig. S2A). Interestingly, loss of SFXN1 markedly reduced M+5 proline released into media to levels similar to those found in PYCR1/2 double knockout cells (Fig. 2B). To test whether loss of SFXN1 reduces labeled proline excretion due to lower labeling of upstream metabolites, independent of its effect on mitochondrial proline release, we assessed labeling of pyrroline-5-carboxylic acid (P5C) from $^{13}C_5$-L-glutamine and found no difference in M+5 P5C in SFXN1 knockout cells, even in the absence of PYCR3 (Fig. 2C). Surprisingly, loss of all PYCR enzymes was required to completely inhibit M+5 proline release, whereas loss of PYCR3 in cells lacking SFXN1 had minimal effect (Fig. 2B). These data suggest that PYCR3 is capable of producing proline in the cytosol when PYCR1/2 are absent, and that other mitochondrial proline transporters may compensate for loss of SFXN1. In support of this, cells lacking PYCR1/2, SFXN1, or SFXN1/PYCR3 can still proliferate in the absence of proline, whereas PYCR1/2/3 triple knockout cells are proline auxotrophs (Fig. 2D).

Since recent studies reported that sideroflexins regulate the assembly of other mitochondrial protein complexes (*25*, *26*), we considered the possibility that loss of SFXN1 indirectly reduces proline export by altering the levels of other mitochondrial transporters. To test this idea, we used quantitative proteomics to look for changes in protein levels in cells lacking SFXN1, and also cells lacking SFXN4, which has a known role in Complex I assembly (*26*). While loss of SFXN4 reduced the levels of Complex I proteins (Fig. S2B-C) as previously described (*26*), no significant protein level changes were detected in SFXN1 knockout cells other than SFXN1 itself (Fig. S2D).

We next wanted to determine whether SFXN1 regulates proline metabolism in a more physiologically relevant setting. In humans, one source of proline is dietary glutamine, which is metabolized to proline within enterocytes of the small intestine (*27*). To study the effects of SFXN1 loss on mitochondrial proline metabolism in this context, we generated SFXN1 knockout intestinal organoids using mice harboring a conditional SFXN1 allele, which was deleted with Cre recombinase expression (Fig. S2E). When incubated with $^{13}C_5$-L-glutamine, organoids lacking SFXN1 released markedly less M+5 proline (Fig. 2E).

Polar neutral amino acids accumulate in SFXN1-null mitochondria

SFXN1 has a known role in mitochondrial serine transport (*9*). Given our findings that SFXN1 also appears to be involved in mitochondrial proline transport, we hypothesized SFXN1 might be involved in transporting other substrates across mitochondrial membranes. To explore this possibility, we immunopurified mitochondria (*28*) from SFXN1 knockout and control cells (Fig. S3A) and measured metabolites using LC-MS. Surprisingly, proline levels were similar in immunopurified mitochondria from control and SFXN1 knockout cells (Fig. S3B), possibly due to increased release of upstream metabolites involved in proline synthesis, such as glutamate, which can be exported from mitochondria through multiple known transporters (*8*). In support of this, SFXN1 and PYCR1/2 knockout cells excreted increased amounts of M+5 glutamate produced from $^{13}C_5$-L-glutamine (Fig. S3C). Nevertheless, levels of several polar neutral amino acids were found to be elevated in SFXN1 knockout mitochondria, including hypotaurine, which is consistent with previous data (*29*), as well as elevated asparagine, glycine, β-alanine, taurine and threonine (Fig. 3A).

The buildup of polar neutral amino acids in SFXN1 knockout mitochondria may reflect a role for SFXN1 in transport of this class of substrates. Indeed, mitochondria isolated from SFXN1 knockout cells demonstrated decreased mitochondrial membrane permeability to these amino acids using mitochondrial swelling assays (Fig. 3B-F), but not the nonpolar neutral amino acid alanine (Fig. S3D). Since serine undergoes conversion to glycine predominantly within mitochondria via SHMT2 (*30*, *31*), we were surprised that loss of a mitochondrial serine transporter resulted in elevated mitochondrial glycine. We hypothesized that compensation by other SFXN isoforms, such as SFXN2 expressed by HEK293T cells, might provide an alternative route for serine transport (*9*). In line with this, loss of SFXN1 only mildly reduced mitochondrial swelling in response to serine (Fig. S3E), while concomitant loss of SFXN1 and SFXN2 led to a larger decrease (Fig. S3F-G).

To test whether SFXN1 is involved in mitochondrial glycine export, we cultured cells with $^{13}C_3$-L-serine, which like glutamine is net consumed (*32*) and can be converted into glycine by cytosolic SHMT1 or mitochondrial SHMT2 (*33*), and measured glycine released into media by LC-MS. Loss of SFXN1 completely inhibited M+2 glycine secretion (Fig. 3G). Interestingly, over-expression of SFXN2 or SFXN3 were able to partially rescue M+2 glycine secretion in SFXN1 null cells (Fig. 3G), while over-expression of SFXN4 or SFXN5 had no effect, which correlated with their ability to rescue mitochondrial swelling in response to glycine (Fig. 3H). While it is possible that lower M+2 glycine secretion could be due to lower mitochondrial serine levels, we observed increased levels of serine in SFXN1 knockout immunopurified mitochondria (Fig. S3H). Another explanation could be that SFXN1 regulates SHMT2 activity independent of a role in direct serine/glycine transport. However, while the SHMT inhibitor SHIN2 (*34*) completely blocked M+2 glycine production from $^{13}C_3$-L-serine (Fig. S3I), it had no effect on mitochondrial serine or glycine swelling (Fig. S3J-K).

Loss of SFXN1 reduces mitochondrial GABA permeability

Solute carriers often transport multiple chemically similar substrates (*35*). Most plasma membrane transporters for proline, glycine, taurine, and β-alanine are members of the SLC6 family, which in humans contains 19 plasma membrane carriers divided among 3 classes: amino acid, monoamine, and GABA transporters (*36*). Since the monoamines serotonin, dopamine, and noradrenaline are synthesized in the cytosol (*37*), and their degradation occurs on the cytosolic side of the outer mitochondrial membrane (*38*), it is unlikely mitochondrial transport of these neurotransmitters is relevant. In contrast, ABAT, the rate-limiting enzyme in GABA degradation localizes to the mitochondrial matrix (*39*). Furthermore, the GABA and amino acid transporters within the SLC6 family demonstrate significant overlapping substrate promiscuity (*36*), and carrier-dependent GABA transport into mitochondria has been described in rat brain (*40*), although the identity of the mammalian mitochondrial GABA transporter has not been reported. To test if SFXN1 is involved in mitochondrial GABA transport, we isolated mitochondria from SFXN1 knockout cells and determined whether GABA-induced swelling was affected. Compared to WT mitochondria, a large reduction in GABA swelling was observed with loss of SFXN1 (Fig. 4A). Importantly, while we observed a slight decrease in membrane potential in the absence of SFXN1 (Fig. S4A), GABA swelling was not altered when mitochondria were uncoupled by FCCP treatment (Fig. S4B-C), consistent with earlier studies demonstrating the mitochondrial transport of most neutral amino acids is insensitive to membrane potential (*11*, *16*, *41*, *42*).

To examine the effects of SFXN1 loss on GABA metabolism, we expressed ABAT in HEK293T cells (Fig. S4D), exposed the cells to $^{13}C_4$-GABA and assessed downstream TCA cycle metabolite labeling via the GABA shunt (Fig. 4B), a well-conserved pathway in both eukaryotic and prokaryotic cells (*43*). ABAT expression increased M+4 malate and M+4 aspartate levels in HEK293T cells after adding $^{13}C_4$-GABA (Fig. S4E), which was sensitive to the ABAT-specific inhibitor Vigabatrin (*44*) (Fig. 4C). Knockout of SFXN1 inhibited ABAT-dependent labeling from $^{13}C_4$-GABA, which was increased by over-expression of SFXN5, and slightly by SFXN2 (Fig. 4D-E), indicating these paralogs may also influence mitochondrial GABA transport. In support of this, over-expression of SFXN2 and SFXN5 also increased GABA swelling in SFXN1 knockout mitochondria, while SFXN3 and SFXN4 had no effect (Fig. 4F).

GABA is the primary inhibitory neurotransmitter in humans and is synthesized in presynaptic neurons and metabolized in glial cells (*7*). To determine the expression level and cell type specificity of these SFXN paralogs in GABAergic regions of the brain, we analyzed single nuclear RNA sequencing data obtained from human and mouse striatum (*45*), which predominantly contains GABAergic medium spiny neurons (*46*), and compared their gene expression profiles to other known GABA metabolic enzymes and transporters. While SFXN1 and SFXN2 are expressed in many cell types within the striatum, SFXN5 expression is largely restricted to astrocytes (Fig. S5), which are responsible for recycling synaptic GABA through ABAT (*7*). This finding is consistent with previous studies demonstrating SFXN5 is an astrocyte-specific marker (*47*, *48*).

Discussion

Many enzymatic reactions in eukaryotes are compartmentalized in mitochondria. Consequently, metabolites must be transported across the inner mitochondrial membrane to coordinate metabolism in the mitochondria with reactions in the cytosol. Using mitochondrial swelling and metabolite profiling, we identify the sideroflexins as enablers of mitochondrial transport of several polar neutral amino acids, including proline, glycine, serine, threonine, β-alanine, hypotaurine, taurine, and GABA. While our data suggest that sideroflexins are required for these amino acids to efficiently cross the mitochondrial inner membrane, we do not provide evidence that they are direct carriers, although this has been reported for serine (*9*). However, it is unlikely that SFXN1 is acting as a chaperone for another carrier since levels of mitochondrial transporters were unaffected by loss of SFXN1. Interestingly, SFXN4, which has a reported role as a chaperone for complex I mitochondrial proteins (*26*), did not rescue any transport defect induced by loss of SFXN1, consistent with its evolutionary divergence from the other sideroflexins (*9*).

We found that loss of SFXN1 reduces mitochondrial proline permeability and inhibits mitochondrial proline export in multiple systems. Interestingly, we also found that loss of mitochondrial proline synthesis did not reduce cell proliferation in the absence of exogenous proline, indicating that proliferation-based screens would be ineffective at identifying mitochondrial proline transporters. Mitochondrial proline synthesis has been shown to support cancer cell proliferation by acting as an alternative electron acceptor (*22*), and also supports collagen synthesis (*49*) and desmoplasia from cancer-associated fibroblasts (*4*), which can limit delivery of cancer therapeutics (*50*). In addition, some cancers may be sensitive to dietary proline restriction (*51*). Upregulation of SFXN1 has been found in breast (*52*) and lung (*53*) cancer, and this is associated with poor prognosis (*53*, *54*). These findings may be due, in part, to SFXN1s role in proline transport, although a disruption of other mitochondrial metabolic pathways might also contribute to this phenotype. For instance, loss of SFXN1 also inhibits mitochondrial transport of both serine and glycine, which impairs one-carbon metabolism and nucleotide synthesis (*9*). Furthermore, we have demonstrated that loss of SFXN1 lowers mitochondrial GABA permeability and inhibits GABA catabolism, and low GABA levels are also predictive of poor prognosis in breast cancer (*55*), while the growth of cells isolated from breast cancer-brain metastases are sensitive to Vigabatrin (*56*).

Loss of SFXN1 predicts a poor outcome in hepatocellular carcinoma and inhibits toxicity induced by a high-fat diet (*57*). This may be due to an inhibitory effect on reactive oxygen

species generation (*57*), since loss of SFXN1 also protects cells from ferroptosis inducers leading to mitochondrial accumulation of taurine and hypotaurine (*29*), which could prevent ferroptosis by acting as antioxidants (*29*, *58–60*). Indeed, apoptosis due to ROS generation by complex I in taurine deficient mice can be rescued with a mitochondrial antioxidant (*61*). Our data suggest that hypotaurine and taurine might accumulate in SFXN1 knockout mitochondria due to decreased export, providing a potential mechanistic link between SFXN1 loss and ferroptosis resistance, which like apoptosis, can be inhibited by mitochondrial ROS quenching (*62*).

We found that SFXN1 loss inhibited isotopically labeled glycine secretion from cells cultured in isotopically labeled serine, in line with previous studies (*9*, *63*). However, we also found that loss of SFXN1 impairs mitochondrial glycine permeability, which could be rescued by SFXN2 and SFXN3, indicating these proteins also regulate mitochondrial glycine transport. Since SFXN1 was reported as synthetic lethal with loss of cytosolic SHMT1 in media lacking serine (*9*), it is possible this phenotype arose from reductions in both mitochondrial serine export and glycine import, since both processes are needed for providing cytosolic serine through mitochondrial SHMT2. Furthermore, loss of function mutations in SFXN1 result in anemia (*64*), likely due to impaired heme biosynthesis (*25*, *65*). Since mitochondrial glycine is required for heme biosynthesis (*66*), our data suggest that these mutations might impair heme synthesis due to impaired mitochondrial glycine or serine availability. Interestingly, loss of function mutations in SLC25A38 also result in anemia (*67*), and complete loss of SLC25A38 sensitizes cells to low vitamin B6 which is required for both ALAS (*68*) and SHMT (*69*) activity, while mitochondrial glycine permeability remains unaffected (*63*).

The only mitochondrial GABA transporter that has been characterized is from plants (*70*), and while a mutation in aralar was identified that led to an increase in the cytoplasmic/mitochondrial GABA ratio in flies, there was no evidence that mitochondrial GABA transport was altered (*71*), and the recombinant AGC isoforms from flies and humans lack GABA transport activity (*72*). We find loss of SFXN1 results in a mitochondrial GABA transport defect that impairs GABA degradation, which can be rescued by SFXN5, and partially by SFXN2. SFXN2 is expressed predominantly in the kidney, while SFXN1 and SFXN5 are expressed throughout the brain (*9*). SFXN5 expression is largely restricted to astrocytes (*47*, *48*), including in the striatum which contains predominantly GABAergic neurons (*46*). Since astrocytes regulate synaptic GABA levels through mitochondrial recycling (*7*), drugs targeting SFXN5 could be effective in treating disorders associated with dysregulated GABAergic transmission, such as epilepsy which is currently treated with the plasma membrane GABA transporter 1 (GAT1) inhibitor Tigabine (*73*) and the ABAT inhibitor Vigabatrin (*74*). Furthermore, we also found that striatal astrocytes and neurons also express SFXN1 and SFXN2, and neurons may also contribute to GABA recycling (*7*).

Lower levels of SFXN1 are found in the brains of Alzheimer's patients (*75*) as well as rats that had undergone ovariectamy (*76*), and a P-element insertion in the fly sideroflexin orthologue enhanced Tau-mediated toxicity (*75*). Since Alzheimer's and ovariectomy are associated with dysregulated GABAergic neurotransmission (*77*, *78*), decreased SFXN1 could disrupt GABA homeostasis. However, SFXN1 might also influence these conditions through regulation of other amino acids. Glycine and β-alanine are neurotransmitters, and taurine, proline, and serine have known neuromodulating properties (*79*). Since these amino acids are found throughout the body,

including GABA (*80*), future studies are needed to determine how mitochondrial metabolism influences the levels of these amino acids in different tissues and to what extent the sideroflexins are involved.

Materials and Methods

Reagents

Antibodies for SFXN1 (HPA019543), and SFXN2 (HPA026834) were obtained from Atlas Antibodies, FLAG (F1804), and Actin (MAB1501) from Sigma-Aldrich, β-Tubulin (2146), β-Actin (D6A8), Vinculin (E1E9V), and Citrate Synthase (CS) (D7V8B) from Cell Signaling Technology, PYCR3 (OTI1B12) from Novus Biologicals, SFXN1 (12296-1-AP), PYCR1 (13108-1-AP), and PYCR2 (17146) from Proteintech, SFXN4 (PA5-35980) from Invitrogen, and Cytochrome C (Cyt C) (ab13575) from Abcam. Horseradish peroxidase–coupled anti-mouse and anti-rabbit secondary antibody were obtained from Cell Signaling Technologies. For cell culture, DMEM (10-017-CV), RPMI (15-040-CV), and penicillin/streptomycin (30-002-CI) were obtained from Corning, FreeStyle 293 Expression Medium (12338018) was obtained from Gibco, and DMEM without glucose, glutamine, serine, glycine, sodium pyruvate (D9802-01) was obtained from United States Biological. For crypt culture media, Advanced DMEM (12491015), and GlutaMAX (35050061) were obtained from Gibco, EGF (315-09), Noggin (250-38), and R-Spondin (315-32) were obtained from Peprotech, *N*-acetyl-L-cysteine (A9165) and Y-27632 dihydrochloride monohydrate (Y0503) were obtained from Sigma-Aldrich, B27 (17504044) was obtained from Life Technologies, and Chir99021 (C-6556) was obtained from LC Laboratories. For crypt embedding, growth factor reduced Matrigel (356231) was obtained from Corning. Pierce anti-HA Magnetic Beads (88837) were obtained from Thermo Scientific. $^{13}C_5$-L-Glutamine and $^{13}C_4$-GABA were obtained from Cambridge Isotope Laboratories and all other amino acids, ammonium chloride, FCCP, rotenone, TMRE, potassium EDTA, polybrene, Tris, Sucrose, magnesium chloride, and potassium chloride were obtained from Sigma-Aldrich. Vigabatrin was obtained from Cayman Chemical Company. (Rac)-SHIN2 was obtained from MedChem Express. For transfection, X-tremeGENE 9 was obtained from Roche, Lipofectamine 3000 obtained from Invitrogen, and TransIT-Lenti Transfection Reagent was obtained from Mirus Bio. For LC-MS, HPLC grade water was obtained from Sigma-Aldrich, and HPLC ultra gradient acetonitrile was obtained from Avantor. For cloning, NEB stable competent cells, T4 DNA ligase, BbsI, Esp3I, T4 Polynucleotide Kinase, T4 Ligation Buffer, CutSmart Buffer, and Shrimp Alkaline Phosphatase were obtained from New England Biolabs.

Cell lines and plasmids

HEK293T and K562 cells were obtained from ATCC. HEK293T cells were used for virus production. ABAT Lentiviral Vector (Human) (CMV) (pLenti-GIII-CMV) (110070610195) was obtained from abm. The plasmids lentiCRISPRv2-Opti (#163126), pSpCas9(BB)-2A-GFP (PX458) (#48138), pU6-(BbsI)_CBh-Cas9-T2A-BFP (#64323), pMXs_FLAG-SFXN1 (#110634), pMXs_FLAG-SFXN2 (#110636), pMXs_FLAG-SFXN3 (#110637), pMXs_FLAG-SFXN4 (#110638), pMXs_FLAG-SFXN5 (#110639), pMXs-bleoR-MitoTag (#218415), pCMV-VSV-G (#8454), pCL-Eco (#12371), pLV hU6-sgRNA hUbC-dCas9-KRAB-T2a-Puro (#71236), pMDLg/pRRE (#12251), pRSV-Rev (#12253), and pMD2.G (#12259) were obtained from Addgene.

Cell culture

HEK293T cells were passaged in DMEM (10-017-CV) supplemented with 10% fetal bovine serum (FBS), penicillin/streptomycin and Plasmocin® Prophylactic. K562 cells were passaged in RPMI (15-040-CV) supplemented with 10% FBS, 2 mM glutamine and penicillin/streptomycin. For isolating mitochondria for swelling assays, HEK293T cells were grown in suspension in FreeStyle 293 Expression Medium (12338018) supplemented with 1% FBS and penicillin/streptomycin, and K562 cells were grown in suspension in RPMI (15-040-CV) supplemented with 5% FBS, 2mM glutamine, 0.1% Pluronic and penicillin/streptomycin.

Generation and culture of organoids from Short Conditional intrON (SCON) SFXN1-floxed mice

The SCON SFXN1-floxed mice were generated via microinjection of mice zygotes at the 1-cell stage (*81*) For microinjection, 25 µl of CRISPR injection mix was prepared in nuclease-free buffer (10 mM TRIS-HCl, pH 7.4 and 0.25 mM EDTA), consisting of spCas9 mRNA (100 ng/µl), spCas9 protein (50 ng/µl), sgRNA (50 ng/µl), and ssODN (20 ng/µl, GenScript). The mixture was centrifuged at 13,000 × g at 4 °C for 15–20 min to prevent the clogging of the injection needles. Intestinal organoids were isolated from the resulting mice and cultured in crypt media consisting of Advanced DMEM supplemented with 1x GlutaMAX, 40 ng/ml EGF, 200 ng/ml Noggin, 500 ng/ml R-Spondin, 1 µM *N*-acetyl-L-cysteine, 1x B27, 1 µM Chir99021, and 10 µM Y-27632 dihydrochloride monohydrate as previously described (*82*).

Virus production and transduction

For lentivirus production, HEK293T cells at 80% confluency were transfected with pMDLg/pRRE, pRSV-Rev, pMD2.G, and one of the following: ABAT Lentiviral Vector (Human) (CMV) (pLenti-GIII-CMV), lentiCRISPRv2-Opti, or pLV hU6-sgRNA hUbC-dCas9-KRAB-T2a-Puro with TransIT-Lenti Transfection Reagent. After 48 hours, the virus-containing media was passed through a 0.45 µm filter and stored at −80 °C. For lentiviral transduction, 200,000 HEK293T cells were seeded in 2 mL of culture medium per well in 6-well plates, and after 24 hours the medium was replaced with 1 mL of virus-containing medium. After 24 hours, virus-containing medium was removed and cells expanded into 10 cm plates. 24 hours later, cells were selected with puromycin. Retroviral production and transduction with pMXs plasmids was performed as previously described (*63*). Briefly, HEK293T cells were spinfected with retrovirus at 1,200 x g for 45 min at 37 °C. After 18 hours, virus was removed and cells were expanded. Selection medium was added 48 hours post-transduction.

The following oligonucleotides were cloned into lentiCRISPRv2-Opti to generate the cells used in the mitochondrial swelling screen:

sgSLC25A16 (1): 5'-CACCGCGGACCCTAACCATGTCAAG-3'
sgSLC25A16 (2): 5'-AAACCTTGACATGGTTAGGGTCCGC-3'
sgSLC25A30 (1): 5'-CACCGTGCCTGGCGTAACATCGCGG-3'
sgSLC25A30 (2): 5'-AAACCCGCGATGTTACGCCAGGCAC-3'
sgSLC25A35 (1): 5'-CACCGGAGGAACCGACGATAACTCG-3'
sgSLC25A35 (2): 5'-AAACCGAGTTATCGTCGGTTCCTCC-3'
sgSLC25A38 (1): 5'-CACCGGAGGAGCATCTATCACAGTG-3'
sgSLC25A38 (2): 5'-AAACCACTGTGATAGATGCTCCTCC-3'

sgSLC25A53 (1): 5'-CACCGTAAAGTTGGAAACGGCCCCA-3'
sgSLC25A53 (2): 5'-AAACTGGGGCCGTTTCCAACTTTAC-3'
sgSFXN1 (1): 5'-CACCGGTTCCCATTCTCATCCGTGA-3'
sgSFXN1 (2): 5'-AAACTCACGGATGAGAATGGGAACC-3'
sgSFXN2 (1): 5'-CACCGCAGATACAAAGACAGTGCGG-3'
sgSFXN2 (2): 5'-AAACCCGCACTGTCTTTGTATCTGC-3'
sgSFXN3 (1): 5'-CACCGGGGCACAAATCTGCCGACCA-3'
sgSFXN3 (2): 5'-AAACTGGTCGGCAGATTTGTGCCCC-3'
sgSFXN4 (1): 5'-CACCGACGGACTTGATCCCTTTCAG-3'
sgSFXN4 (2): 5'-AAACCTGAAAGGGATCAAGTCCGTC-3'
sgSFXN5 (1): 5'-CACCGCAGTGACAAAGAGTGTGCGA-3'
sgSFXN5 (2): 5'-AAACTCGCACACTCTTTGTCACTGC-3'
sgNTC (1): 5'-CACCGTAACCGATACTCCCCACATT-3'
sgNTC (2): 5'-AAACAATGTGGGGAGTATCGGTTAC-3'

The following oligonucleotides were cloned into pLV hU6-sgRNA hUbC-dCas9-KRAB-T2a-Puro and used with SFXN1$^{-/-}$ HEK239T cells to generate new lines lacking both SFXN1 and either PYCR3 or SFXN2:

sgPYCR3 (1): CACCGCGGCGTCCGAGGCAACAAGA
sgPYCR3 (2): AAACTCTTGTTGCCTCGGACGCCGC
sgSFXN2 (1): CACCGGTAACTGGTGGCATTTGTCC
sgSFXN2 (2): AAACGGACAAATGCCACCAGTTACC

Generation of CRISPR knockout cells

Knockout lines were generated using a previously described protocol (*83*). Briefly, HEK293T or K562 cells were transfected with pSpCas9(BB)-2A-GFP (PX458) or pU6-(BbsI)_CBh-Cas9-T2A-BFP containing guides of interest. 48 hours later, BFP/GFP positive cells were single cell sorted into 96 well plates and expanded to establish clonal lines. Knockout of genes of interest were confirmed by western blot.

The following oligonucleotides were cloned into either pSpCas9(BB)-2A-GFP (PX458) or pU6-(BbsI)_CBh-Cas9-T2A-BFP to generate clonal knockout lines:

sgSFXN1 (1): 5'-CACCGTCTTCACTGTAACTGACCCC-3'
sgSFXN1 (2): 5'-AAACGGGGTCAGTTACAGTGAAGAC-3'
sgSFXN4 (1): 5'-CACCGGCGCACGTTGGGCTCAATGA-3'
sgSFXN4 (2): 5'-AAACTCATTGAGCCCAACGTGCGCC-3'
sgPYCR1 (1A): 5'-CACCGAGAGCCGGTGCCATCTGTGG-3'
sgPYCR1 (2A): 5'-AAACCCACAGATGGCACCGGCTCTC-3'
sgPYCR1 (1B): 5'-CACCGCTGCTGTGAAGCCCTTGGCC-3'
sgPYCR1 (2B): 5'-AAACGGCCAAGGGCTTCACAGCAGC-3'
sgPYCR2 (1A): 5'-CACCGGATGGTGACACCAGCCGCAC-3'
sgPYCR2 (2A): 5'-AAACGTGCGGCTGGTGTCACCATCC-3'
sgPYCR2 (1B): 5'-CACCGGAACCTGACACGCAGCAACA-3'
sgPYCR2 (2B): 5'-AAACTGTTGCTGCGTGTCAGGTTCC-3'

sgPYCR3 (1A): 5'-CACCGTGGATGGGCGGTGAGCGCAG-3'
sgPYCR3 (2A): 5'-AAACCTGCGCTCACCGCCCATCCAC-3'
sgPYCR3 (1B): 5'-CACCGCCCACGAAGCCCACGCGCCG-3'
sgPYCR3 (2B): 5'-AAACCGGCGCGTGGGCTTCGTGGGC-3'

PYCR1/2 and PYCR 1/2/3 knockout lines were generated using 2 guides per gene

Immunoblotting

Cell immunoblots were performed as previously described (*84*). Briefly, cells were washed 1x in PBS and lysed in RIPA buffer containing protease inhibitors. Proteins were resolved using SDS-PAGE and transferred to nitrocellulose membranes for immunoblotting using the iBlot2 Dry Blotting System (Thermo Fisher). The blots were blocked for 1 hour in TBST with 5% (w/v) non-fat dry milk. Antibodies were also used in TBST with 5% (w/v) non-fat dry milk. Primary antibodies were used at 1:1000 dilution, and HRP-linked secondary antibodies were used at 1:5000 dilution. After imaging, blots were treated with a stripping reagent followed by hydrogen peroxide treatment, and then re-blocked and re-probed for other proteins according to a previously described protocol (*85*). Organoid immunoblots were performed using a similar protocol, except blots were blocked in TBST with 5% FBS, SFXN1 was detected using 12296-1-AP (for cell immunoblots HPA019543 was used to detect SFXN1), and proteins were probed on separate blots.

Mitochondrial isolation and swelling assay

Isolation of mitochondria and the swelling assay were carried out using a previously described protocol (*63*). Briefly, 1x 10^9 cells were washed with cold PBS and resuspended in cold isolation buffer (250 mM sucrose, 10 mM Tris pH 7.5, 10 mM KCl, 1.5 mM $MgCl_2$, 1 mM potassium EDTA). Cells were lysed on ice using 30 strokes with a dounce homogenizer and tight fit pestle, and mitochondria were isolated by differential centrifugation. Mitochondria were diluted to 2 mg/mL in room temperature swelling buffer (20 mM Tris pH 7.5, 0.5 mM potassium EDTA, 10 μM rotenone) and incubated at room temperature for 30 minutes before swelling was initiated by adding an equal volume of room temperature swelling buffer containing 500 mM substrate (250 mM final concentration). Swelling was monitored by measuring absorbance at 520 nm using a microplate reader, and swelling rates were determined as the absolute value of the change in absorbance at 520 nm from 0 to 90 seconds. Swelling rates were normalized to simultaneously swollen WT mitochondria unless otherwise stated.

Assessment of proliferation and TMRE staining

For proliferation experiments, 50,000 HEK293T cells were seeded per well in Poly-D-Lysine coated 6-well plates in 2 mL of DMEM (10-017-CV) supplemented with 10% dialyzed FBS and penicillin/streptomycin. 16 hours later the media was removed and cells were washed 1x with PBS and incubated in fresh media supplemented with either vehicle or 1 mM proline. Separately plated cells were also counted at this time point using a Cellometer Auto T4 Plus Cell Counter (Nexcelcom Bioscience). 48 hours later, cells were counted again and doublings were determined as $\log_2$ fold change between the counts. For TMRE staining, TMRE fluorescence measurements were performed using a previously described protocol (*86*). Briefly, HEK293T cells were incubated in DMEM (10-017-CV) supplemented with 10% dialyzed FBS,

penicillin/streptomycin, and 150 nM TMRE for 5 minutes at room temperature. Fluorescence was then measured by flow cytometry using a 561 nm laser.

Isotope labeled metabolite tracing

For $^{13}C_5$-L-glutamine tracing into media metabolite measurements, 200,000 HEK293T cells were seeded per well in Poly-D-Lysine coated 6-well plates in 2 mL of DMEM (17-207-CV) supplemented with 4.5 g/L glucose, 2mM L-glutamine, 10% dialyzed FBS, and penicillin/streptomycin. For $^{13}C_5$-L-glutamine tracing into whole cell metabolites, 400,000 cells were used. 16 hours later the media was removed and cells were washed 1x with PBS and incubated in fresh media with 2mM L-glutamine substituted with 2mM $^{13}C_5$-L-glutamine. For media, 24 hours after addition of label, 15 µL of media was collected and briefly vortexed with 150 µL of extraction buffer (HPLC grade 80% methanol 20% water containing isotopically labeled amino acid standards). For whole cell metabolite quantification, cells were washed 1x with cold blood bank saline at the indicated time points and lysed with 400 µL of cold extraction buffer and vortexed at 4°C for 10 minutes. Both media and whole cell samples were then centrifuged at 20,000 x g for 10 minutes to remove insoluble material. The supernatant was then filtered through a 10 kDa PES filter and metabolites were quantified by LC-MS. Peak areas were normalized to an isotopically labeled internal amino acid standard to yield area ratios, and these ratios were normalized to cell counts performed using a Cellometer Auto T4 Plus Cell Counter (Nexcelcom Bioscience) on separately plated cells that were treated with identical experimental conditions. $^{13}C_3$-L-serine tracing was performed using the same protocol, except cells were cultured in DMEM (D9802-01) supplemented with 4.5 g/L glucose, 3.7 g/L sodium bicarbonate, 2mM L-glutamine, 400 µM L-serine, 10% dialyzed FBS, and penicillin/streptomycin. For tracing media, 400 µM L-Serine was substituted with 400 µM $^{13}C_3$-L-Serine. For $^{13}C_5$-L-glutamine tracing in organoids, intestinal crypts organoids were isolated and cultured in crypt culture medium for 48 hours, and then placed into fresh media with 1x GlutaMAX substituted with 0.2 mM $^{13}C_5$-L-glutamine. After 24 hours 15µl of media was added to 150 µl of extraction buffer which was briefly vortexed and centrifuged at 20,000 x g for 10 minutes. The supernatant was then filtered through a 10 kDa PES filter and metabolites were quantified by LC-MS. Peak areas were normalized to an isotopically labeled internal amino acid standard to yield area ratios, and these ratios were normalized to total organoid protein determined by BCA. For $^{13}C_4$-GABA tracing, 400,000 HEK293T cells were seeded per well in Poly-D-Lysine coated 6-well plates in 2 mL of DMEM (10-017-CV) supplemented with 10% dialyzed FBS and penicillin/streptomycin. 16 hours later the media was removed and cells were washed 1x with PBS, and cells were incubated in fresh media supplemented with 1mM GABA. 24 hours later, the cells were washed 1x with PBS and fresh media was added with 1mM GABA substituted with 1mM $^{13}C_4$-GABA. Cells were washed 1x with cold blood bank saline at the indicated time points and lysed with 400 µL of cold extraction buffer and vortexed at 4°C for 10 minutes. Samples were then centrifuged at 20,000 x g for 10 minutes to remove insoluble material. The supernatant was then filtered through a 10 kDa PES filter and metabolites were quantified by LC-MS. Peak areas were normalized to an isotopically labeled internal amino acid standard to yield area ratios, and these ratios were normalized to cell counts using separately plated cells that were treated with identical experimental conditions.

Immunopurification of mitochondria

Mitochondria were immunopurified for metabolomics using a protocol adapted from previous studies (*28*, *63*, *87*). 10x 10^6 HEK293T cells were seeded in 150 mm plates in 20 mL of DMEM (10-017-CV) supplemented with 10% FBS and penicillin/streptomycin. 16 hours later the plates were placed on ice, media was removed and cells were scraped into 5 mL of cold KPBS and centrifuged at 250 x g for 3 minutes. All following steps were performed at 4°C. Cell pellets were resuspended in 1 mL of KPBS and lysed with 10 strokes using a syringe attached to a 26G needle and centrifuged at 1100 x g for 2 minutes. 5 µl of supernatant was taken for input immunoblotting, and the rest was rotated with 100 µl of KPBS-equilibrated pierce anti-HA-magnetic beads for 5 minutes. The beads were then bound to a magnet and washed 3x with 1 mL KPBS. Before the third wash was removed, 5 µl was taken for IP immunoblotting. 100 µl of extraction buffer was then added and the beads were vortexed for 10 minutes. The beads were then magnet removed, and excess beads and insoluble material were removed by centrifugation at 20,000 x g for 10 minutes. The supernatant was collected and analyzed by LC-MS. For volcano plot analysis, peak areas were normalized to the summed peak areas of all internal isotopic amino acid standards, which was then normalized to Cytochrome C levels determined by immunoblot densitometry. Statistical analysis for targeted metabolomics was performed using MetaboAnalyst 6.0 operating on one factor default settings (*88*). For reporting individual metabolites, peak areas were normalized to an isotopically labeled internal amino acid standard to yield area ratios, and these ratios were normalized to Cytochrome C levels determined by immunoblot densitometry.

LC–MS metabolite measurements

Polar metabolite profiling was performed using a previously described protocol (*89*). Briefly, LC–MS was carried out using a QExactive orbitrap mass spectrometer equipped with a Dionex Ultimate 3000 UPLC system (Thermofisher). All samples were injected onto a SeQuant ZIC-pHILIC 2.1 mm × 150 mm (5 µm particle size) column (Millipore Sigma), and chromatography was performed starting with 20% buffer A (20 mM ammonium carbonate, 0.1% ammonium hydroxide), and 80% acetonitrile. A chromatographic gradient of linearly decreasing acetonitrile concentration was used with the mass spectrometer operating in full scan, polarity-switching mode. Metabolite identification was determined by referencing a library of chemical standards which was constructed using external standard pools (*90*), and relative quantification of metabolites was carried out using XCalibur 2.2 software (Thermo Fisher Scientific).

Quantitative LC/MS proteomics

Mitochondria in isolation buffer or whole cells washed 3x with cold PBS were flash frozen in liquid nitrogen and stored at -80°C. Tandem mass tag MS was carried out by the Thermo Fisher Scientific Center for Multiplexed Proteomics at Harvard Medical School (https://tcmp.hms.harvard.edu). Samples for protein analysis were prepared essentially as previously described (*91*, *92*). Proteomes (from whole cells or isolated mitochondria) were extracted using a buffer containing 200 mM EPPS pH 8.5, 8M urea, 0.1% SDS and protease inhibitors. Following lysis, ~150 µg of each sample was reduced with 5 mM TCEP. Cysteine residues were alkylated using 10 mM iodoacetimide for 20 minutes at RT in the dark. Excess iodoacetimide was quenched with 10 mM DTT. A buffer exchange was carried out using a modified SP3 protocol (*93*). ~1500 µg of Cytiva SpeedBead Magnetic Carboxylate Modified Particles (65152105050250 and 4515210505250), mixed at a 1:1 ratio, were added to each sample. 100% ethanol was added to each sample to achieve a final ethanol concentration of at

least 50%. Samples were incubated with gentle shaking for 15 mins. Samples were washed three times with 80% ethanol. Protein was eluted from SP3 beads using 200 mM EPPS pH 8.5 containing Lys-C (1:50: Wako, 129-02541) and incubated overnight at room temperature. Samples were further digested with trypsin (1:50; ThermoFisher Scientific, 90305R20) at 37°C with vigorous shaking. Acetonitrile was added to each sample to achieve a final concentration of ~33%. Each sample was labelled, in the presence of SP3 beads, with ~360 µg of TMTPro 16-plex reagents (ThermoFisher Scientific). Following confirmation of satisfactory labelling (>97%), excess TMT was quenched by addition of hydroxylamine to a final concentration of 0.3%. The full volume from each sample was pooled and acetonitrile was removed by vacuum centrifugation for 1 hour. The pooled sample was acidified using formic acid and peptides were de-salted using a Sep-Pak 50mg tC18 cartridge (Waters). Peptides were eluted in 70% acetonitrile, 1% formic acid and dried by vacuum centrifugation. The TMT labeled peptides were solubilized in 5% ACN/10 mM ammonium bicarbonate, pH 8.0 and ~300 µg of TMT labeled peptides were separated by an Agilent 300 Extend C18 column (3.5 µm particles, 4.6 mm ID and 250 mm in length). An Agilent 1260 binary pump coupled with a photodiode array (PDA) detector (Thermo Scientific) was used to separate the peptides. A 45-minute linear gradient from 10% to 40% acetonitrile in 10 mM ammonium bicarbonate pH 8.0 (flow rate of 0.6 mL/min) separated the peptide mixtures into a total of 96 fractions (36 seconds). A total of 96 Fractions were consolidated into 24 samples in a checkerboard fashion and vacuum dried to completion. Each sample was desalted via Stage Tips and re-dissolved in 5% FA/ 5% ACN for LC-MS3 analysis. Proteome data were collected on an Orbitrap Fusion Lumos mass spectrometer (ThermoFisher Scientific) coupled to a Proxeon EASY-nLC 1000 LC pump (ThermoFisher Scientific). Fractionated peptides were separated using a 120 min gradient at 550 nL/min on a 35 cm column (i.d. 100 µm, Accucore, 2.6 µm, 150 Å) packed in-house. MS1 data were collected in the Orbitrap (120,000 resolution; maximum injection time 50 ms; AGC 6×10^5). Charge states between 2 and 6 were required for MS2 analysis, and a 120 s dynamic exclusion window was used. Top 10 MS2 scans were performed in the ion trap with CID fragmentation (isolation window 0.5 Da; Rapid; NCE 35%; maximum injection time 50 ms; AGC 1.5×10^4). An on-line real-time search algorithm (Orbiter) was used to trigger MS3 scans for quantification (*94*). MS3 scans were collected in the Orbitrap using a resolution of 50,000, NCE of 55%, maximum injection time of 200 ms, and AGC of 3.0×10^5. The close out was set at two peptides per protein per fraction (*94*). Raw files were converted to mzXML, and monoisotopic peaks were re-assigned using Monocle (*95*). Searches were performed using the Comet search algorithm against a human database downloaded from Uniprot in May 2021. A 50 ppm precursor ion tolerance, 1.0005 fragment ion tolerance, and 0.4 fragment bin offset for MS2 scans collected in the ion trap. TMTpro on lysine residues and peptide N-termini (+304.2071 Da) and carbamidomethylation of cysteine residues (+57.0215 Da) were set as static modifications, while oxidation of methionine residues (+15.9949 Da) was set as a variable modification. Each run was filtered separately to 1% False Discovery Rate (FDR) on the peptide-spectrum match (PSM) level. Then proteins were filtered to the target 1% FDR level across the entire combined data set. For reporter ion quantification, a 0.003 Da window around the theoretical m/z of each reporter ion was scanned, and the most intense m/z was used. Reporter ion intensities were adjusted to correct for isotopic impurities of the different TMTpro reagents according to manufacturer specifications. Peptides were filtered to include only those with a summed signal-to-noise (SN) ≥ 160 across all TMT channels. The signal-to-noise (S/N) measurements of peptides assigned to each protein were summed (for a given protein). These values were

normalized so that the sum of the signal for all proteins in each channel was equivalent thereby accounting for equal protein loading. For volcano plots only proteins with ≥ 3 peptides were reported.

Statistical analysis

Two tailed t-tests were used for comparing differences between two groups, and Analysis of Variance (ANOVA) followed by either Šídák's or Dunnett's multiple comparison tests was used for comparing differences between more than two groups. $p < 0.05$ was considered statistically significant, and most analyses and plots were generated using GraphPad PRISM 9.

References

1. C. N. Cunningham, J. Rutter, 20,000 picometers under the OMM: diving into the vastness of mitochondrial metabolite transport. *EMBO Rep.* **21**, e50071 (2020).

2. D. A. Pious, P. Hawley, Effect of antibiotics on respiration in human cells. *Pediatr. Res.* **6**, 687–692 (1972).

3. E. Kummer, N. Ban, Mechanisms and regulation of protein synthesis in mitochondria. *Nat. Rev. Mol. Cell Biol.* **22**, 307–325 (2021).

4. E. J. Kay, K. Paterson, C. Riera-Domingo, D. Sumpton, J. H. M. Däbritz, S. Tardito, C. Boldrini, J. R. Hernandez-Fernaud, D. Athineos, S. Dhayade, E. Stepanova, E. Gjerga, L. J. Neilson, S. Lilla, A. Hedley, G. Koulouras, G. McGregor, C. Jamieson, R. M. Johnson, M. Park, K. Kirschner, C. Miller, J. J. Kamphorst, F. Loayza-Puch, J. Saez-Rodriguez, M. Mazzone, K. Blyth, M. Zagnoni, S. Zanivan, Cancer-associated fibroblasts require proline synthesis by PYCR1 for the deposition of pro-tumorigenic extracellular matrix. *Nat. Metab.* **4**, 693–710 (2022).

5. G. W. Crabtree, A. J. Park, J. A. Gordon, J. A. Gogos, Cytosolic Accumulation of L-Proline Disrupts GABA-Ergic Transmission through GAD Blockade. *Cell Rep.* **17**, 570–582 (2016).

6. Y. Yao, W. Han, Proline Metabolism in Neurological and Psychiatric Disorders. *Mol. Cells* **45**, 781–788 (2022).

7. J. V. Andersen, A. Schousboe, Milestone Review: Metabolic dynamics of glutamate and GABA mediated neurotransmission — The essential roles of astrocytes. *J. Neurochem.* **166**, 109–137 (2023).

8. M. Monné, A. Vozza, F. M. Lasorsa, V. Porcelli, F. Palmieri, Mitochondrial Carriers for Aspartate, Glutamate and Other Amino Acids: A Review. *Int. J. Mol. Sci.* **20**, 4456 (2019).

9. N. Kory, G. A. Wyant, G. Prakash, J. uit de Bos, F. Bottanelli, M. E. Pacold, S. H. Chan, C. A. Lewis, T. Wang, H. R. Keys, Y. E. Guo, D. M. Sabatini, SFXN1 is a mitochondrial serine transporter required for one-carbon metabolism. *Science* **362**, eaat9528 (2018).

10. J. Meyer, Proline transport in rat liver mitochondria. *Arch. Biochem. Biophys.* **178**, 387–395 (1977).

11. R. L. Cybulski, R. R. Fisher, Mitochondrial neutral amino acid transport: evidence for a carrier mediated mechanism. *Biochemistry* **16**, 5116–5120 (1977).

12. C. Di Martino, R. Pizzuto, M. L. Pallotta, A. De Santis, S. Passarella, Mitochondrial transport in proline catabolism in plants: the existence of two separate translocators in mitochondria isolated from durum wheat seedlings. *Planta* **223**, 1123–1133 (2006).

13. M. L. Pallotta, l-Proline uptake in Saccharomyces cerevisiae mitochondria can contribute to bioenergetics during nutrient stress as alternative mitochondrial fuel. *World J. Microbiol. Biotechnol.* **30**, 19–31 (2014).

14. A. Atlante, S. Passarella, P. Pierro, E. Quagliariello, Proline transport in rat kidney mitochondria. *Arch. Biochem. Biophys.* **309**, 139–148 (1994).

15. J. B. Chappell, Systems used for the transport of substrates into mitochondria. *Br. Med. Bull.* **24**, 150–157 (1968).

16. K. F. LaNoue, A. C. Schoolwerth, Metabolite transport in mitochondria. *Annu. Rev. Biochem.* **48**, 871–922 (1979).

17. K. D. Garlid, A. D. Beavis, Swelling and contraction of the mitochondrial matrix. II. Quantitative application of the light scattering technique to solute transport across the inner membrane. *J. Biol. Chem.* **260**, 13434–13441 (1985).

18. A. D. Beavis, R. D. Brannan, K. D. Garlid, Swelling and contraction of the mitochondrial matrix. I. A structural interpretation of the relationship between light scattering and matrix volume. *J. Biol. Chem.* **260**, 13424–13433 (1985).

19. N. E. Sanjana, O. Shalem, F. Zhang, Improved vectors and genome-wide libraries for CRISPR screening. *Nat. Methods* **11**, 783–784 (2014).

20. P. Lunetti, F. Damiano, G. De Benedetto, L. Siculella, A. Pennetta, L. Muto, E. Paradies, C. M. T. Marobbio, V. Dolce, L. Capobianco, Characterization of Human and Yeast Mitochondrial Glycine Carriers with Implications for Heme Biosynthesis and Anemia. *J. Biol. Chem.* **291**, 19746–19759 (2016).

21. J. De Ingeniis, B. Ratnikov, A. D. Richardson, D. A. Scott, P. Aza-Blanc, S. K. De, M. Kazanov, M. Pellecchia, Z. Ronai, A. L. Osterman, J. W. Smith, Functional specialization in proline biosynthesis of melanoma. *PloS One* **7**, e45190 (2012).

22. R. L. Westbrook, E. Bridges, J. Roberts, C. Escribano-Gonzalez, K. L. Eales, L. A. Vettore, P. D. Walker, E. Vera-Siguenza, H. Rana, F. Cuozzo, K.-L. Eskla, H. Vellama, A. Shaaban, C. Nixon, H. Luuk, G. G. Lavery, D. J. Hodson, A. L. Harris, D. A. Tennant, Proline synthesis through PYCR1 is required to support cancer cell proliferation and survival in oxygen-limiting conditions. *Cell Rep.* **38**, 110320 (2022).

23. D. H. Tran, R. Kesavan, H. Rion, M. H. Soflaee, A. Solmonson, D. Bezwada, H. S. Vu, F. Cai, J. A. Phillips, R. J. DeBerardinis, G. Hoxhaj, Mitochondrial NADP+ is essential for proline biosynthesis during cell growth. *Nat. Metab.* **3**, 571–585 (2021).

24. J. Zhu, S. Schwörer, M. Berisa, Y. J. Kyung, K. W. Ryu, J. Yi, X. Jiang, J. R. Cross, C. B. Thompson, Mitochondrial NADP(H) generation is essential for proline biosynthesis. *Science* **372**, 968–972 (2021).

25. M. G. Acoba, E. S. S. Alpergin, S. Renuse, L. Fernández-del-Río, Y.-W. Lu, O. Khalimonchuk, C. F. Clarke, A. Pandey, M. J. Wolfgang, S. M. Claypool, The mitochondrial carrier SFXN1 is critical for complex III integrity and cellular metabolism. *Cell Rep.* **34**, 108869 (2021).

26. T. D. Jackson, J. J. Crameri, L. Muellner-Wong, A. E. Frazier, C. S. Palmer, L. E. Formosa, D. H. Hock, K. M. Fujihara, T. Stait, A. J. Sharpe, D. R. Thorburn, M. T. Ryan, D. A. Stroud, D. Stojanovski, Sideroflexin 4 is a complex I assembly factor that interacts with the MCIA complex and is required for the assembly of the ND2 module. *Proc. Natl. Acad. Sci.* **119**, e2115566119 (2022).

27. M. Watford, Glutamine metabolism and function in relation to proline synthesis and the safety of glutamine and proline supplementation. *J. Nutr.* **138**, 2003S-2007S (2008).

28. W. W. Chen, E. Freinkman, T. Wang, K. Birsoy, D. M. Sabatini, Absolute Quantification of Matrix Metabolites Reveals the Dynamics of Mitochondrial Metabolism. *Cell* **166**, 1324-1337.e11 (2016).

29. M. Soula, R. A. Weber, O. Zilka, H. Alwaseem, K. La, F. Yen, H. Molina, J. Garcia-Bermudez, D. A. Pratt, K. Birsoy, Metabolic determinants of cancer cell sensitivity to canonical ferroptosis inducers. *Nat. Chem. Biol.* **16**, 1351–1360 (2020).

30. A. S. Tibbetts, D. R. Appling, Compartmentalization of Mammalian folate-mediated one-carbon metabolism. *Annu. Rev. Nutr.* **30**, 57–81 (2010).

31. C. A. Lewis, S. J. Parker, B. P. Fiske, D. McCloskey, D. Y. Gui, C. R. Green, N. I. Vokes, A. M. Feist, M. G. Vander Heiden, C. M. Metallo, Tracing compartmentalized NADPH metabolism in the cytosol and mitochondria of mammalian cells. *Mol. Cell* **55**, 253–263 (2014).

32. G. D. Stoner, D. J. Merchant, Amino acid utilization by L-M strain mouse cells in a chemically defined medium. *In Vitro* **7**, 330–343 (1972).

33. A. C. Newman, O. D. K. Maddocks, One-carbon metabolism in cancer. *Br. J. Cancer* **116**, 1499–1504 (2017).

34. J. C. García-Cañaveras, O. Lancho, G. S. Ducker, J. M. Ghergurovich, X. Xu, V. da Silva-Diz, S. Minuzzo, S. Indraccolo, H. Kim, D. Herranz, J. D. Rabinowitz, SHMT inhibition is effective and synergizes with methotrexate in T-cell acute lymphoblastic leukemia. *Leukemia* **35**, 377–388 (2021).

35. P. Kandasamy, G. Gyimesi, Y. Kanai, M. A. Hediger, Amino acid transporters revisited: New views in health and disease. *Trends Biochem. Sci.* **43**, 752–789 (2018).

36. S. Bröer, U. Gether, The solute carrier 6 family of transporters. *Br. J. Pharmacol.* **167**, 256–278 (2012).

37. K. L. Sims, G. A. Davis, F. E. Bloom, Activities of 3,4-dihydroxy-L-phenylalanine and 5-hydroxy-L-tryptophan decarboxylases in rat brain: assay characteristics and distribution. *J. Neurochem.* **20**, 449–464 (1973).

38. C. Schnaitman, V. G. Erwin, J. W. Greenawalt, The submitochondrial localization of monoamine oxidase. An enzymatic marker for the outer membrane of rat liver mitochondria. *J. Cell Biol.* **32**, 719–735 (1967).

39. I. Schousboe, B. Bro, A. Schousboe, Intramitochondrial localization of the 4-aminobutyrate-2-oxoglutarate transaminase from ox brain. *Biochem. J.* **162**, 303–307 (1977).

40. S. Passarella, A. Atlante, M. Barile, E. Quagliariello, Carrier mediated GABA translocation into rat brain mitochondria. *Biochem. Biophys. Res. Commun.* **121**, 770–778 (1984).

41. J. Benavides, M. L. Garcia, J. Lopez-Lahoya, M. Ugarte, F. Valdivieso, Glycine transport in rat brain and liver mitochondria. *Biochim. Biophys. Acta BBA - Biomembr.* **598**, 588–594 (1980).

42. M. D. Brand, J. B. Chappell, Permeability of Mitochondria from Rat Brain and Rat Liver to Gaba. *J. Neurochem.* **22**, 47–51 (1974).

43. N. Bouché, B. Lacombe, H. Fromm, GABA signaling: a conserved and ubiquitous mechanism. *Trends Cell Biol.* **13**, 607–610 (2003).

44. M. J. Jung, B. Lippert, B. W. Metcalf, P. Böhlen, P. J. Schechter, gamma-Vinyl GABA (4-amino-hex-5-enoic acid), a new selective irreversible inhibitor of GABA-T: effects on brain GABA metabolism in mice. *J. Neurochem.* **29**, 797–802 (1977).

45. A. Matsushima, S. S. Pineda, J. R. Crittenden, H. Lee, K. Galani, J. Mantero, G. Tombaugh, M. Kellis, M. Heiman, A. M. Graybiel, Transcriptional vulnerabilities of striatal neurons in human and rodent models of Huntington's disease. *Nat. Commun.* **14**, 282 (2023).

46. L. M. Yager, A. F. Garcia, A. M. Wunsch, S. M. Ferguson, The ins and outs of the striatum: Role in drug addiction. *Neuroscience* **301**, 529–541 (2015).

47. C. Fecher, L. Trovò, S. A. Müller, N. Snaidero, J. Wettmarshausen, S. Heink, O. Ortiz, I. Wagner, R. Kühn, J. Hartmann, R. M. Karl, A. Konnerth, T. Korn, W. Wurst, D. Merkler, S. F. Lichtenthaler, F. Perocchi, T. Misgeld, Cell-type-specific profiling of brain mitochondria reveals functional and molecular diversity. *Nat. Neurosci.* **22**, 1731–1742 (2019).

48. J. A. Stokum, B. Shim, W. Huang, M. Kane, J. A. Smith, V. Gerzanich, J. M. Simard, A large portion of the astrocyte proteome is dedicated to perivascular endfeet, including critical components of the electron transport chain. *J. Cereb. Blood Flow Metab.* **41**, 2546–2560 (2021).

49. S. Schwörer, M. Berisa, S. Violante, W. Qin, J. Zhu, R. C. Hendrickson, J. R. Cross, C. B. Thompson, Proline biosynthesis is a vent for TGFβ-induced mitochondrial redox stress. *EMBO J.* **39**, e103334 (2020).

50. N. D. Ebelt, V. Zamloot, E. R. Manuel, Targeting desmoplasia in pancreatic cancer as an essential first step to effective therapy. *Oncotarget* **11**, 3486–3488 (2020).

51. N. Sahu, D. Dela Cruz, M. Gao, W. Sandoval, P. M. Haverty, J. Liu, J.-P. Stephan, B. Haley, M. Classon, G. Hatzivassiliou, J. Settleman, Proline Starvation Induces Unresolved ER Stress and Hinders mTORC1-Dependent Tumorigenesis. *Cell Metab.* **24**, 753–761 (2016).

52. L. Andriani, Y.-X. Ling, S.-Y. Yang, Q. Zhao, X.-Y. Ma, M.-Y. Huang, Y.-L. Zhang, F.-L. Zhang, D.-Q. Li, Z.-M. Shao, Sideroflexin-1 promotes progression and sensitivity to lapatinib in triple-negative breast cancer by inhibiting TOLLIP-mediated autophagic degradation of CIP2A. *Cancer Lett.* **597**, 217008 (2024).

53. L. Chen, Y. Kang, Y. Jiang, J. You, C. Huang, X. Xu, F. Chen, Overexpression of SFXN1 indicates poor prognosis and promotes tumor progression in lung adenocarcinoma. *Pathol. Res. Pract.* **237**, 154031 (2022).

54. D. Yuan, J. Liu, W. Sang, Q. Li, Comprehensive analysis of the role of SFXN family in breast cancer. *Open Med. Wars. Pol.* **18**, 20230685 (2023).

55. A. Brzozowska, F. Burdan, D. Duma, J. Solski, M. Mazurkiewicz, γ-amino butyric acid (GABA) level as an overall survival risk factor in breast cancer. *Ann. Agric. Environ. Med. AAEM* **24**, 435–439 (2017).

56. J. Neman, J. Termini, S. Wilczynski, N. Vaidehi, C. Choy, C. M. Kowolik, H. Li, A. C. Hambrecht, E. Roberts, R. Jandial, Human breast cancer metastases to the brain display GABAergic properties in the neural niche. *Proc. Natl. Acad. Sci.* **111**, 984–989 (2014).

57. K. Yagi, S. Shimada, Y. Akiyama, M. Hatano, D. Asano, Y. Ishikawa, H. Ueda, S. Watanabe, K. Akahoshi, H. Ono, M. Tanabe, S. Tanaka, Loss of SFXN1 mitigates lipotoxicity and predicts poor outcome in non-viral hepatocellular carcinoma. *Sci. Rep.* **13**, 9449 (2023).

58. O. I. Aruoma, B. Halliwell, B. M. Hoey, J. Butler, The antioxidant action of taurine, hypotaurine and their metabolic precursors. *Biochem. J.* **256**, 251–255 (1988).

59. H. Xiao, X. Du, Z. Tao, N. Jing, S. Bao, W. Gao, B. Dong, Y. Fang, Taurine Inhibits Ferroptosis Mediated by the Crosstalk between Tumor Cells and Tumor-Associated Macrophages in Prostate Cancer. *Adv. Sci.* **11**, 2303894 (2023).

60. B. Tadolini, G. Pintus, G. G. Pinna, F. Bennardini, F. Franconi, Effects of taurine and hypotaurine on lipid peroxidation. *Biochem. Biophys. Res. Commun.* **213**, 820–826 (1995).

61. C. J. Jong, T. Ito, H. Prentice, J.-Y. Wu, S. W. Schaffer, Role of Mitochondria and Endoplasmic Reticulum in Taurine-Deficiency-Mediated Apoptosis. *Nutrients* **9**, 795 (2017).

62. S.-J. Oh, M. Ikeda, T. Ide, K. Y. Hur, M.-S. Lee, Mitochondrial event as an ultimate step in ferroptosis. *Cell Death Discov.* **8**, 1–13 (2022).

63. I. A. Pena, J. S. Shi, S. M. Chang, J. Yang, S. Block, C. H. Adelmann, H. R. Keys, P. Ge, S. Bathla, I. H. Witham, G. Sienski, A. C. Nairn, D. M. Sabatini, C. A. Lewis, N. Kory, M. G. Vander Heiden, M. Heiman, SLC25A38 is required for mitochondrial pyridoxal 5'-phosphate (PLP) accumulation. *Nat. Commun.* **16**, 978 (2025).

64. M. D. Fleming, D. R. Campagna, J. N. Haslett, C. C. Trenor, N. C. Andrews, A mutation in a mitochondrial transmembrane protein is responsible for the pleiotropic hematological and skeletal phenotype of flexed-tail (f/f) mice. *Genes Dev.* **15**, 652–657 (2001).

65. B. Bao, W. An, Q. Lu, Y. Wang, Z. Lu, J. Tu, H. Zhang, Y. Duan, W. Yuan, X. Zhu, H. Jia, Sfxn1 is essential for erythrocyte maturation via facilitating hemoglobin production in zebrafish. *Biochim. Biophys. Acta Mol. Basis Dis.* **1867**, 166096 (2021).

66. K. D. Gibson, W. G. Laver, A. Neuberger, Initial stages in the biosynthesis of porphyrins. 2. The formation of δ-aminolaevulic acid from glycine and succinyl-coenzyme A by particles from chicken erythrocytes. *Biochem. J.* **70**, 71–81 (1958).

67. D. L. Guernsey, H. Jiang, D. R. Campagna, S. C. Evans, M. Ferguson, M. D. Kellogg, M. Lachance, M. Matsuoka, M. Nightingale, A. Rideout, L. Saint-Amant, P. J. Schmidt, A. Orr, S. S. Bottomley, M. D. Fleming, M. Ludman, S. Dyack, C. V. Fernandez, M. E. Samuels, Mutations in mitochondrial carrier family gene SLC25A38 cause nonsyndromic autosomal recessive congenital sideroblastic anemia. *Nat. Genet.* **41**, 651–653 (2009).

68. B. M. Stojanovski, G. A. Hunter, I. Na, V. N. Uversky, R. H. Y. Jiang, G. C. Ferreira, 5-Aminolevulinate synthase catalysis: The catcher in heme biosynthesis. *Mol. Genet. Metab.* **128**, 178–189 (2019).

69. K. Snell, U. Baumann, P. C. Byrne, K. J. Chave, S. B. Renwick, P. G. Sanders, S. K. Whitehouse, The genetic organization and protein crystallographic structure of human serine hydroxymethyltransferase. *Adv. Enzyme Regul.* **40**, 353–403 (2000).

70. S. Michaeli, A. Fait, K. Lagor, A. Nunes-Nesi, N. Grillich, A. Yellin, D. Bar, M. Khan, A. R. Fernie, F. J. Turano, H. Fromm, A mitochondrial GABA permease connects the GABA shunt and the TCA cycle, and is essential for normal carbon metabolism. *Plant J.* **67**, 485–498 (2011).

71. A. K. Kanellopoulos, V. Mariano, M. Spinazzi, Y. J. Woo, C. McLean, U. Pech, K. W. Li, J. D. Armstrong, A. Giangrande, P. Callaerts, A. B. Smit, B. S. Abrahams, A. Fiala, T.

Achsel, C. Bagni, Aralar Sequesters GABA into Hyperactive Mitochondria, Causing Social Behavior Deficits. *Cell* **180**, 1178-1197.e20 (2020).

72. V. Porcelli, S. Barile, L. Capobianco, S. N. Barile, R. Gorgoglione, G. Fiermonte, B. Monti, F. M. Lasorsa, L. Palmieri, The mitochondrial aspartate/glutamate carrier does not transport GABA. *Biochim. Biophys. Acta Bioenerg.* **1865**, 149487 (2024).

73. A. Schousboe, P. Wellendorph, B. Frølund, R. P. Clausen, P. Krogsgaard-Larsen, Astrocytic GABA Transporters: Pharmacological Properties and Targets for Antiepileptic Drugs. *Adv. Neurobiol.* **16**, 283–296 (2017).

74. E. Ben-Menachem, Mechanism of action of vigabatrin: correcting misperceptions. *Acta Neurol. Scand.* **124**, 5–15 (2011).

75. B. Minjarez, K. G. Calderón-González, Ma. L. V. Rustarazo, M. E. Herrera-Aguirre, M. L. Labra-Barrios, D. E. Rincon-Limas, M. M. S. del Pino, R. Mena, J. P. Luna-Arias, Identification of proteins that are differentially expressed in brains with Alzheimer's disease using iTRAQ labeling and tandem mass spectrometry. *J. Proteomics* **139**, 103–121 (2016).

76. Y.-Y. Fang, P. Zeng, N. Qu, L.-N. Ning, J. Chu, T. Zhang, X.-W. Zhou, Q. Tian, Evidence of altered depression and dementia-related proteins in the brains of young rats after ovariectomy. *J. Neurochem.* **146**, 703–721 (2018).

77. J. Jiménez-Balado, T. S. Eich, GABAergic dysfunction, neural network hyperactivity and memory impairments in human aging and Alzheimer's disease. *Semin. Cell Dev. Biol.* **116**, 146–159 (2021).

78. M. Jüptner, A. Jussofie, C. Hiemke, Effects of ovariectomy and steroid replacement on GABAA receptor binding in female rat brain. *J. Steroid Biochem. Mol. Biol.* **38**, 141–147 (1991).

79. R. Dalangin, A. Kim, R. E. Campbell, The Role of Amino Acids in Neurotransmission and Fluorescent Tools for Their Detection. *Int. J. Mol. Sci.* **21**, 6197 (2020).

80. S. L. Erdö, J. R. Wolff, gamma-Aminobutyric acid outside the mammalian brain. *J. Neurochem.* **54**, 363–372 (1990).

81. S.-H. S. Wu, H. Lee, R. Szép-Bakonyi, G. Colozza, A. Boese, K. R. Gert, N. Hallay, J.-H. Lee, J. Kim, Y. Zhu, M. M. Linssen, S. Pilat-Carotta, P. Hohenstein, H.-C. Theussl, A. Pauli, B.-K. Koo, SCON—a Short Conditional intrON for conditional knockout with one-step zygote injection. *Exp. Mol. Med.* **54**, 2188–2199 (2022).

82. M. D. Mana, A. M. Hussey, C. N. Tzouanas, S. Imada, Y. B. Millan, D. Bahceci, D. R. Saiz, A. T. Webb, C. A. Lewis, P. Carmeliet, M. M. Mihaylova, A. K. Shalek, Ö. H. Yilmaz, High-fat diet-activated fatty acid oxidation mediates intestinal stemness and tumorigenicity. *Cell Rep.* **35** (2021).

83. A. M. Darnell, A. R. Subramaniam, E. K. O'Shea, Translational Control through Differential Ribosome Pausing during Amino Acid Limitation in Mammalian Cells. *Mol. Cell* **71**, 229-243.e11 (2018).

84. A. Luengo, Z. Li, D. Y. Gui, L. B. Sullivan, M. Zagorulya, B. T. Do, R. Ferreira, A. Naamati, A. Ali, C. A. Lewis, C. J. Thomas, S. Spranger, N. J. Matheson, M. G. Vander Heiden, Increased demand for NAD+ relative to ATP drives aerobic glycolysis. *Mol. Cell* **81**, 691-707.e6 (2021).

85. M. R. Sullivan, A. M. Darnell, M. F. Reilly, T. Kunchok, L. Joesch-Cohen, D. Rosenberg, A. Ali, M. G. Rees, J. A. Roth, C. A. Lewis, M. G. Vander Heiden, Methionine synthase is essential for cancer cell proliferation in physiological folate environments. *Nat. Metab.* **3**, 1500–1511 (2021).

86. L. C. Crowley, M. E. Christensen, N. J. Waterhouse, Measuring Mitochondrial Transmembrane Potential by TMRE Staining. *Cold Spring Harb. Protoc.* **2016**, pdb.prot087361 (2016).

87. W. W. Chen, E. Freinkman, D. M. Sabatini, Rapid immunopurification of mitochondria for metabolite profiling and absolute quantification of matrix metabolites. *Nat. Protoc.* **12**, 2215–2231 (2017).

88. Z. Pang, Y. Lu, G. Zhou, F. Hui, L. Xu, C. Viau, A. F. Spigelman, P. E. MacDonald, D. S. Wishart, S. Li, J. Xia, MetaboAnalyst 6.0: towards a unified platform for metabolomics data processing, analysis and interpretation. *Nucleic Acids Res.* **52**, W398–W406 (2024).

89. C. Chidley, A. M. Darnell, B. L. Gaudio, E. C. Lien, A. M. Barbeau, M. G. Vander Heiden, P. K. Sorger, A CRISPRi/a screening platform to study cellular nutrient transport in diverse microenvironments. *Nat. Cell Biol.* **26**, 825–838 (2024).

90. M. R. Sullivan, L. V. Danai, C. A. Lewis, S. H. Chan, D. Y. Gui, T. Kunchok, E. A. Dennstedt, M. G. Vander Heiden, A. Muir, Quantification of microenvironmental metabolites in murine cancers reveals determinants of tumor nutrient availability. *eLife* **8**, e44235 (2019).

91. J. Navarrete-Perea, Q. Yu, S. P. Gygi, J. A. Paulo, Streamlined Tandem Mass Tag (SL-TMT) Protocol: An Efficient Strategy for Quantitative (Phospho)proteome Profiling Using Tandem Mass Tag-Synchronous Precursor Selection-MS3. *J. Proteome Res.* **17**, 2226–2236 (2018).

92. J. Li, Z. Cai, R. D. Bomgarden, I. Pike, K. Kuhn, J. C. Rogers, T. M. Roberts, S. P. Gygi, J. A. Paulo, TMTpro-18plex: The Expanded and Complete Set of TMTpro Reagents for Sample Multiplexing. *J. Proteome Res.* **20**, 2964–2972 (2021).

93. C. S. Hughes, S. Moggridge, T. Müller, P. H. Sorensen, G. B. Morin, J. Krijgsveld, Single-pot, solid-phase-enhanced sample preparation for proteomics experiments. *Nat. Protoc.* **14**, 68–85 (2019).

94. D. K. Schweppe, J. K. Eng, Q. Yu, D. Bailey, R. Rad, J. Navarrete-Perea, E. L. Huttlin, B. K. Erickson, J. A. Paulo, S. P. Gygi, Full-Featured, Real-Time Database Searching Platform Enables Fast and Accurate Multiplexed Quantitative Proteomics. *J. Proteome Res.* **19**, 2026–2034 (2020).

95. R. Rad, J. Li, J. Mintseris, J. O'Connell, S. P. Gygi, D. K. Schweppe, Improved Monoisotopic Mass Estimation for Deeper Proteome Coverage. *J. Proteome Res.* **20**, 591–598 (2021).

Acknowledgements: We thank all members of the Vander Heiden and Kory labs for thoughtful discussions and feedback; Dr. Jonathan Van Vranken and the Thermo Fisher Scientific Center for Multiplexed Proteomics at Harvard Medical School for performing quantitative proteomics and analysis; and Dr. Michael DeMott and the Bioimaging and Chemical Analysis Facility Core at MIT for support with mass spectrometry instrumentation used for polar metabolomics.

Funding: S.B. was supported by the National Institutes of Health (NIH) (T32GM007287, T32HL007118). M.G.V.H. acknowledges support from the MIT Center for Precision Cancer Medicine, the Ludwig Center at MIT, and the NIH (R35CA242379, P30CA014051). N.K. acknowledges support from the NIH/NCI (R00 CA241332), the Smith Family Awards Program for Excellence in Biomedical Research, Damon Runyon-Dale F. Frey Award (DFS 46-21), and Damon Runyon-Rachleff Innovation Award (73S-22). K.L.A. was supported by the National Science Foundation (DGE-1122374) and NIH (F31CA271787, T32GM007287). M.H. acknowledges support from the NIH (R35NS127327). Figure schematics were created using BioRender.com.

Author Contributions: S.B., F.C., and S.S.P. performed experiments and analyzed data. P.C.R., K.L.A. and A.M.D. provided experimental design and critical supplies. Ö.H.Y., M.H., and I.A.P. provided critical feedback. S.B., N.K. and M.G.V.H. designed the study and wrote the manuscript with input from all authors.

Competing Interests: M.G.V.H. discloses that he is an advisor for Agios Pharmaceuticals, iTeos Therapeutics, MPM Capital, Droia Ventures, Pretzel Therapeutics, Lime Therapeutics, Faeth Therapeutics and Auron Therapeutics. All other authors declare no competing interests.

Data and materials availability: All data are available in either the main text or supplementary materials. Custom biological materials may be obtained by request from the corresponding authors.

Supplementary Materials
Figs. S1 to S5

Figure 1

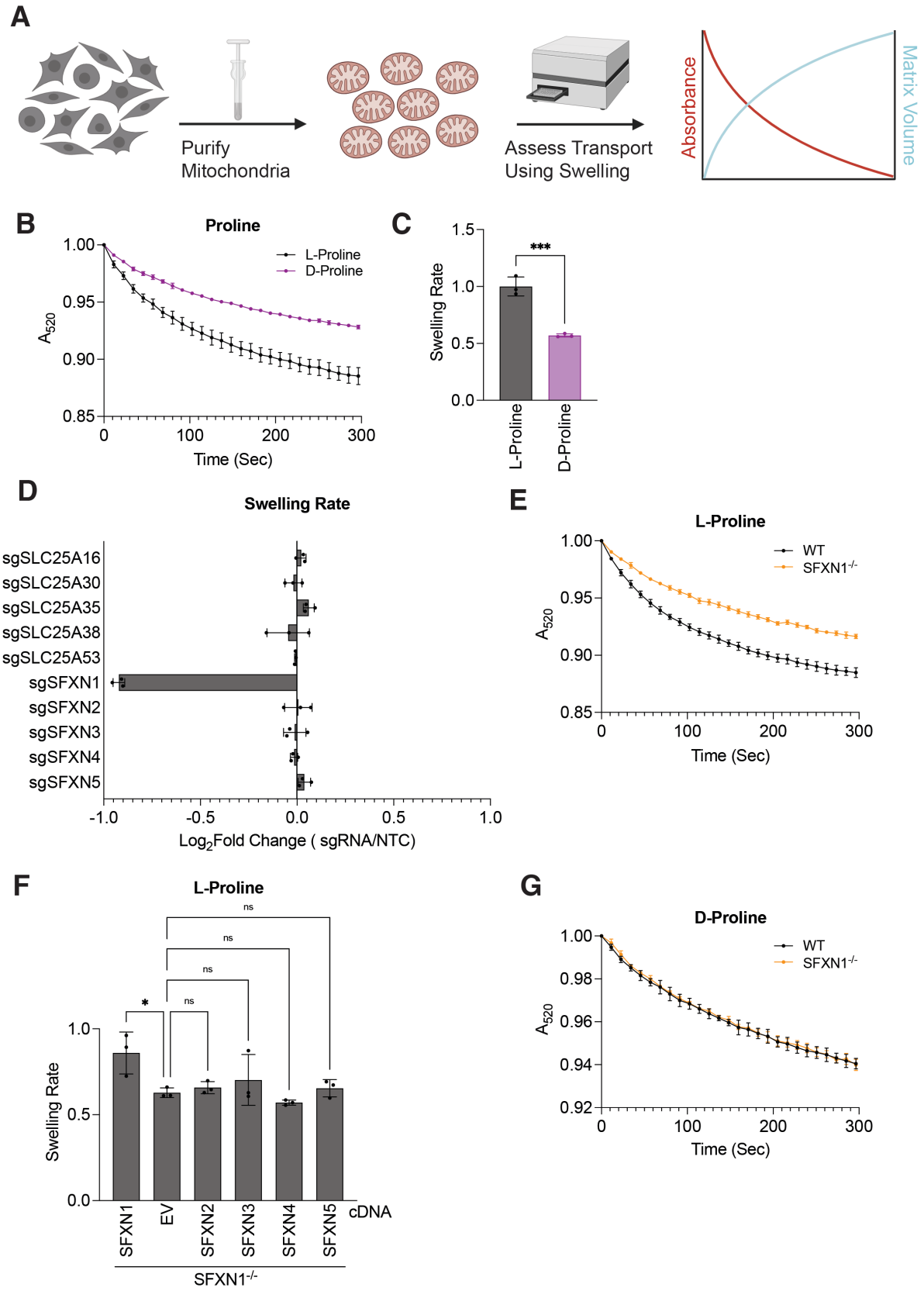
A
Purify
Mitochondria
Assess Transport
Using Swelling
Absorbance
Matrix Volume
B
Proline
L-Proline
D-Proline
A_{520}
Time (Sec)
C
Swelling Rate
***
L-Proline
D-Proline
D
Swelling Rate
sgSLC25A16
sgSLC25A30
sgSLC25A35
sgSLC25A38
sgSLC25A53
sgSFXN1
sgSFXN2
sgSFXN3
sgSFXN4
sgSFXN5
Log_2Fold Change (sgRNA/NTC)
E
L-Proline
WT
SFXN1-/-
A_{520}
Time (Sec)
F
L-Proline
ns
*
Swelling Rate
SFXN1
EV
SFXN2
SFXN3
SFXN4
SFXN5
cDNA
SFXN1-/-
G
D-Proline
WT
SFXN1-/-
A_{520}
Time (Sec)

Fig. 1. Loss of SFXN1 reduces mitochondrial proline permeability. (A) Schematic of mitochondrial swelling experiment to study transport. **(B)** Swelling curves of HEK239T mitochondria treated with either L or D-proline; n=3 ± SD. **(C)** Relative swelling rates of HEK239T mitochondria treated with either L or D-proline derived from data shown in (B). Values were normalized to L-proline; n=3 ± SD, unpaired t-test ***$p < 0.001$. **(D)** Swelling rates of mitochondria treated with L-proline from HEK293T cells expressing guides targeting the indicated candidate transport protein (sgRNA) compared to non-targeting control (NTC) expressing cells; n=3 ± SD. **(E)** Swelling curves of HEK239T mitochondria treated with L-proline from either wild type (WT) or SFXN1 knockout ($SFXN1^{-/-}$) cells; n=3 ± SD. **(F)** Swelling rates of mitochondria treated with L-proline from SFXN1 knockout ($SFXN1^{-/-}$) HEK293T cells expressing the indicated cDNA or empty vector (EV); n=3 ± SD, one-way ANOVA followed by Dunnett's multiple comparisons test *$p < 0.05$, ns = not significant. (**G)** Swelling curves of HEK239T mitochondria treated with D-proline from either wild type (WT) or SFXN1 knockout ($SFXN1^{-/-}$) cells; n=3 ± SD.

Figure 2

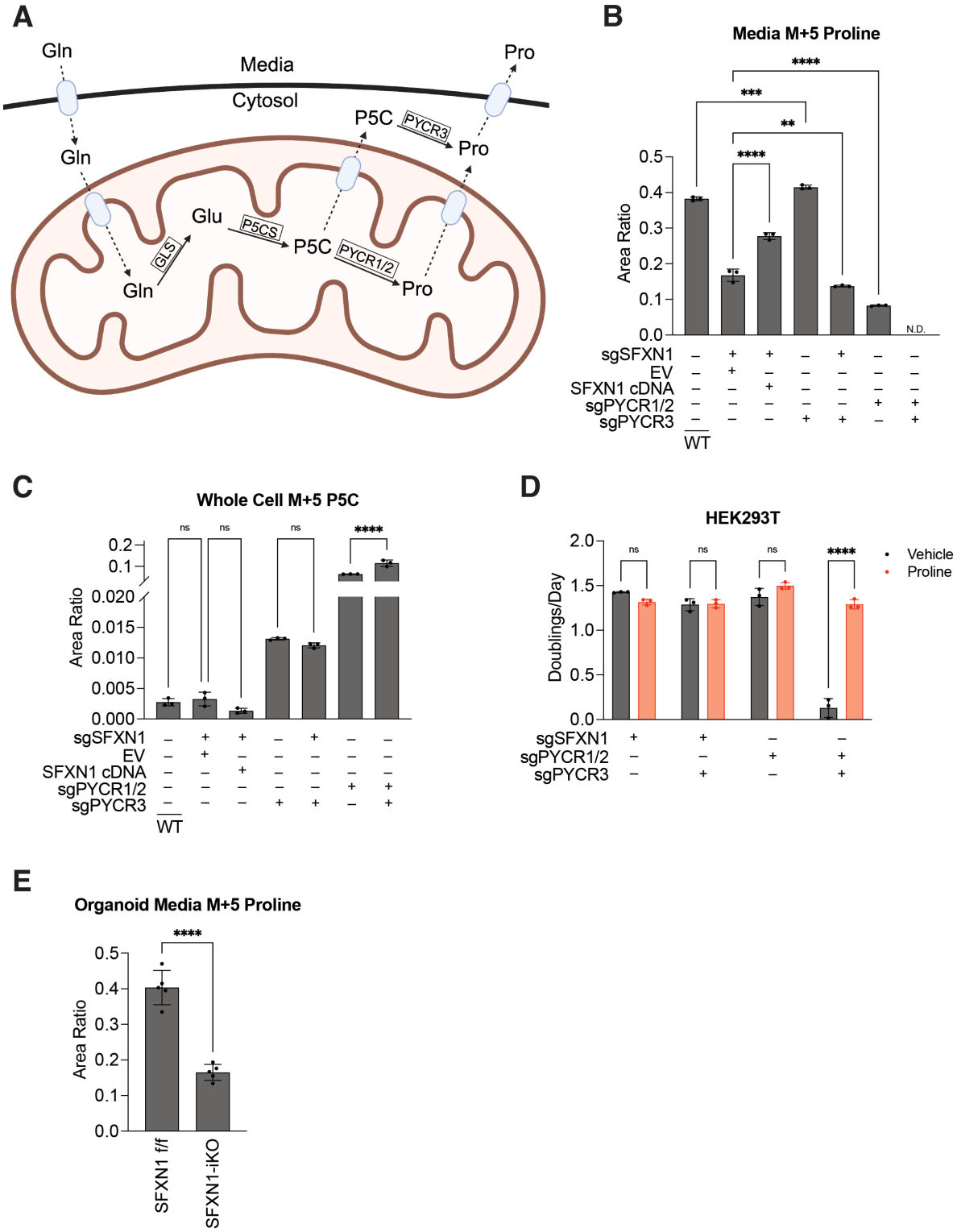
A
Gln
Media
Pro
Cytosol
P5C
PYCR3
Pro
Gln
Glu
P5CS
P5C
PYCR1/2
GLS
Gln
Pro
B
Media M+5 Proline
Area Ratio
N.D.
sgSFXN1
EV
SFXN1 cDNA
sgPYCR1/2
sgPYCR3
WT
C
Whole Cell M+5 P5C
Area Ratio
ns
****
sgSFXN1
EV
SFXN1 cDNA
sgPYCR1/2
sgPYCR3
WT
D
HEK293T
Doublings/Day
Vehicle
Proline
sgSFXN1
sgPYCR1/2
sgPYCR3
E
Organoid Media M+5 Proline
Area Ratio
SFXN1 f/f
SFXN1-iKO

Fig. 2. SFXN1 regulates mitochondrial proline export. (A) Schematic of how compartmentalized glutamine metabolism relates to proline synthesis. **(B)** Relative media M+5 proline levels measured by mass spectrometry from wild type (WT) HEK293T cells and cells depleted of SFXN1 (sgSFXN1) and the indicated PYCR isoforms (sgPYCR), with or without expression of SFXN1 cDNA or empty vector (EV) as indicated, when cultured in $^{13}C_5$-L-glutamine for 24 hours; n=3 ± SD, one-way ANOVA followed by Dunnett's multiple comparisons test $^{**}p < 0.01$, $^{****}p < 0.0001$. **(C)** Relative whole cell M+5 P5C levels measured by mass spectrometry from wild type (WT) HEK293T cells and cells depleted of SFXN1 (sgSFXN1) and the indicated PYCR isoforms (sgPYCR), with or without expression of SFXN1 cDNA or empty vector (EV) as indicated, when cultured in $^{13}C_5$-L-glutamine for 8 hours; n=3 ± SD, one-way ANOVA followed by Šídák's multiple comparisons test $^{****}p < 0.0001$, ns is not significant. **(D)** Proliferation rates of HEK293T cells depleted of SFXN1 (sgSFXN1) and the indicated PYCR isoforms (sgPYCR) cultured in vehicle or 1mM proline for 48 hours; n=3 ± SD, two-way ANOVA followed by Šídák's multiple comparisons test $^{****}p < 0.0001$. **(E)** Relative media M+5 proline levels measured by mass spectrometry from SFXN1 floxed (f/f) and SFXN1 knockout (-iKO) intestinal crypt organoids cultured in $^{13}C_5$-L-glutamine for 24 hours; n=5 ± SD, unpaired t-test $^{****}p < 0.0001$.

Figure 3

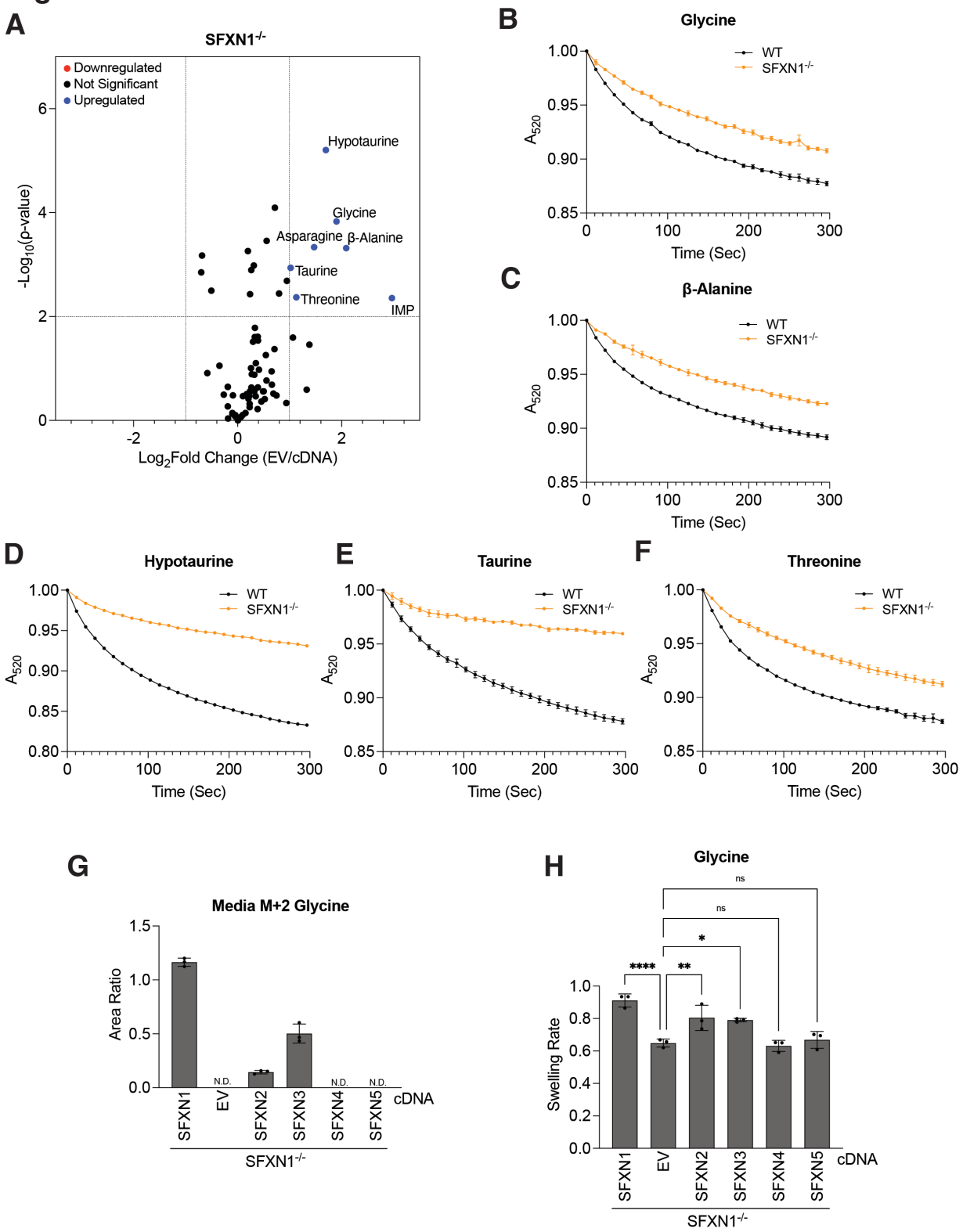
A
SFXN1-/-
Downregulated
Not Significant
Upregulated
Hypotaurine
Glycine
Asparagine
β-Alanine
Taurine
Threonine
IMP
-Log10(p-value)
Log2Fold Change (EV/cDNA)
B
Glycine
WT
SFXN1-/-
A520
Time (Sec)
C
β-Alanine
D
Hypotaurine
E
Taurine
F
Threonine
G
Media M+2 Glycine
Area Ratio
N.D.
SFXN1
EV
SFXN2
SFXN3
SFXN4
SFXN5
cDNA
H
Glycine
ns
*
**
****
Swelling Rate

Fig. 3. SFXN1 regulates mitochondrial permeability of many polar neutral amino acids. (A). Targeted metabolomics of immunopurified mitochondria from SFXN1 knockout ($SFXN1^{-/-}$) HEK293T cells expressing empty vector (EV) compared to SFXN1 knockout cells expressing SFXN1 (cDNA); *n*=3. **(B-F)** Swelling curves of mitochondria treated with the indicated amino acids from wild type (WT) or SFXN1 knockout ($SFXN1^{-/-}$) HEK293T cells; *n*=3 ± SD. **(G)** Relative media M+2 glycine levels measured by mass spectrometry from SFXN1 knockout ($SFXN1^{-/-}$) HEK293T cells expressing the indicated cDNA or empty vector (EV) cultured in $^{13}C_3$-L-Serine for 24 hours; *n*=3 ± SD, N.D. is not detected. **(H)** Swelling rates of mitochondria treated with glycine from SFXN1 knockout ($SFXN1^{-/-}$) HEK293T cells expressing the indicated cDNA or empty vector (EV); *n*=3 ± SD, one-way ANOVA followed by Dunnett's multiple comparisons test $*p < 0.05$, $**p < 0.01$, $****p < 0.0001$, ns is not significant.

Figure 4

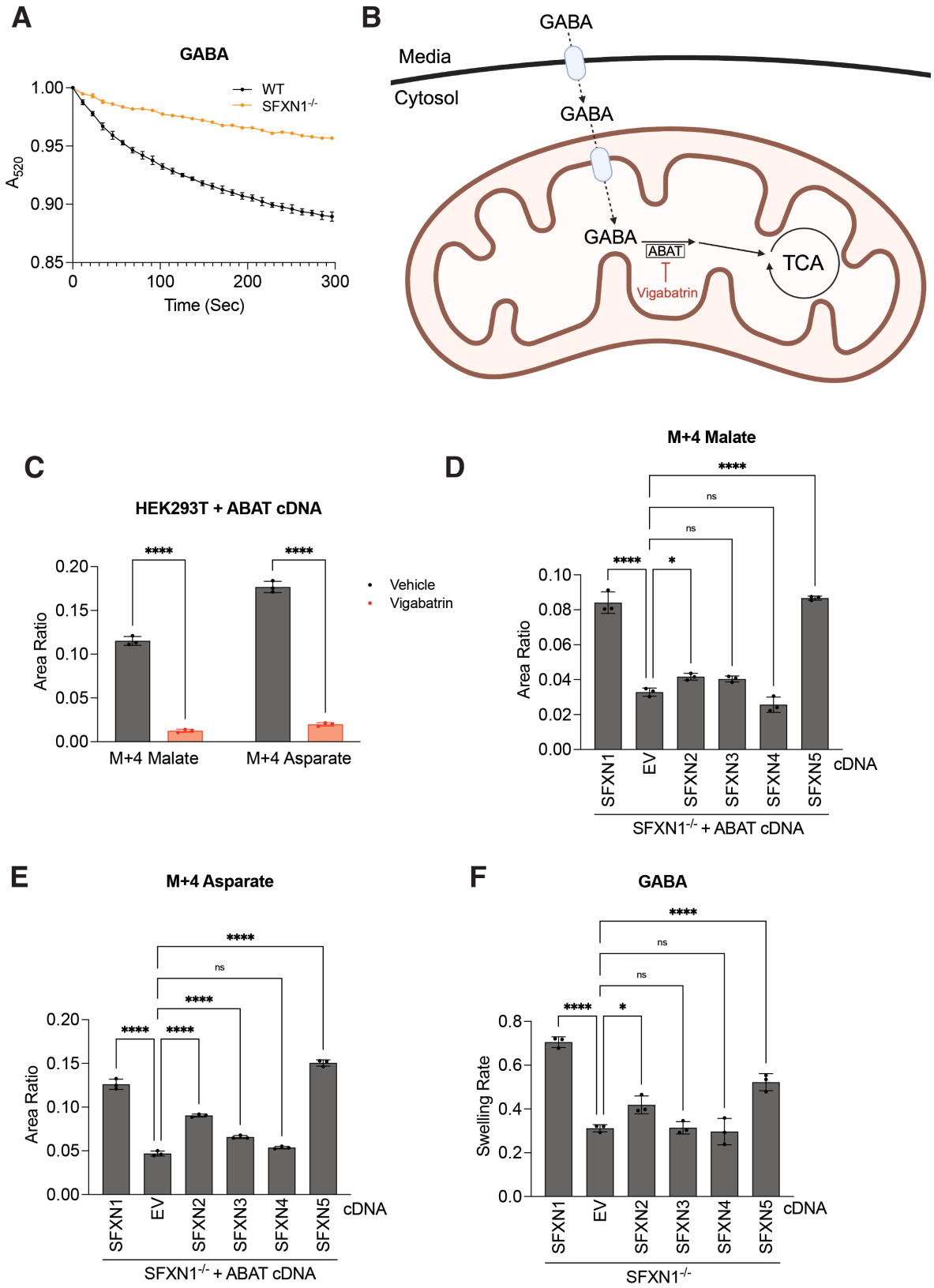
A
GABA
WT
SFXN1-/-
A520
1.00
0.95
0.90
0.85
0
100
200
300
Time (Sec)
B
GABA
Media
Cytosol
GABA
GABA
ABAT
Vigabatrin
TCA
C
HEK293T + ABAT cDNA
Area Ratio
0.20
0.15
0.10
0.05
0.00
****
****
Vehicle
Vigabatrin
M+4 Malate
M+4 Asparate
D
M+4 Malate
****
ns
ns
****
*
Area Ratio
0.10
0.08
0.06
0.04
0.02
0.00
SFXN1
EV
SFXN2
SFXN3
SFXN4
SFXN5
cDNA
SFXN1-/- + ABAT cDNA
E
M+4 Asparate
****
ns
****
****
****
Area Ratio
0.20
0.15
0.10
0.05
0.00
SFXN1
EV
SFXN2
SFXN3
SFXN4
SFXN5
cDNA
SFXN1-/- + ABAT cDNA
F
GABA
****
ns
ns
****
*
Swelling Rate
0.8
0.6
0.4
0.2
0.0
SFXN1
EV
SFXN2
SFXN3
SFXN4
SFXN5
cDNA
SFXN1-/-

Fig. 4. SFXN1 regulates mitochondrial GABA permeability. (A) Swelling curves of HEK293T mitochondria treated with GABA from either wild type (WT) or SFXN1 knockout ($SFXN1^{-/-}$) cells; n=3 ± SD. **(B)** Schematic of mitochondrial GABA metabolism through the matrix localized enzyme ABAT. TCA is tricarboxylic acid cycle. **(C)** Relative M+4 malate and M+4 aspartate levels measured by mass spectrometry from ABAT cDNA-expressing HEK239T cells that were pre-treated with either vehicle (DMSO) or 1mM Vigabatrin for 24 hours and then cultured in $^{13}C_4$-GABA for 30 minutes; n=3 ± SD, two-way ANOVA followed by Šídák's multiple comparisons test ****$p < 0.0001$. **(D-E)** Relative whole cell M+4 malate and M+4 aspartate levels measured by mass spectrometry from ABAT cDNA-expressing SFXN1 knockout ($SFXN1^{-/-}$) HEK239T cells expressing the indicated cDNA or empty vector (EV) cultured in $^{13}C_4$-GABA for 30 minutes. Area ratios were normalized to ABAT levels determined by western blot densitometry; n=3 ± SD, one-way ANOVA followed by Dunnett's multiple comparisons test ***$p = 0.001$, ****$p < 0.0001$, ns is not significant. **(F)** Swelling rates of mitochondria treated with GABA from SFNX1 knockout ($SFXN1^{-/-}$) HEK239T cells expressing the indicated cDNA or empty vector (EV); one-way ANOVA followed by Dunnett's multiple comparisons test *p <0.05, ****$p < 0.0001$, ns is not significant.